

# COMMISSIONING THE SPEAR3 DIAGNOSTIC BEAMLINES<sup>§</sup>

Jeff Corbett, Cecile Limborg-Deprey, Walter Mok and Andy Ringwall,  
SLAC, Menlo Park, USA

## Abstract

SPEAR3 has two diagnostic beam lines: an x-ray pinhole camera and a visible/UV beam line. The pinhole camera images  $\sim 8$  keV dipole synchrotron radiation (SR) incident on a phosphor screen. The visible beam line delivers conventional optical radiation to an array of cameras and diagnostic elements on a 1x3m optical bench. This paper briefly reviews the pinhole camera system while concentrating more on visible beam line power transmission calculations and streak camera data. Impedance estimates in the nominal optics and bunch length measurements in low-alpha optics are presented.

## INTRODUCTION

SPEAR3 first started routine operation in early 2003. Although the SR diagnostics were not available, commissioning proceeded smoothly and the machine performed to specification. By 2004, beam transmission resumed to the (SPEAR2) x-ray pinhole camera. This system has a fixed  $30 \times 25 \mu\text{m}$  rectangular aperture and demagnification factor of about  $M=0.6$ . The detector unit includes Al filters, a 0.56mm YaG plate and a metal-coated Si mirror oriented at  $45^\circ$  to the beam. A Pulnix TM1300 camera connected to a National Instruments framegrabber images the florescent spot via the mirror.

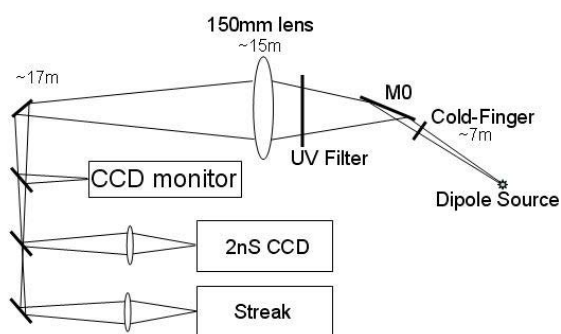


Figure 1: Schematic of the visible/UV beam line.

The visible/UV beam line accepts  $3.5 \times 6 \text{mrad}$  dipole SR through an exit port rendered obsolete by the injection system. A  $\pm 0.6 \text{mrad}$  GlidCop<sup>®</sup> ‘cold-finger’ extends horizontally across the x-ray core of the beam. The remaining beam is deflected  $18^\circ$  horizontally by a flat, Rh-coated Si mirror and propagates unfocused onto the optical bench with a  $50 \times 95 \text{mm}$  rectangular cross-section.

The  $\text{SiO}_2$  vacuum windows transmit photon energies up to about 6eV. At present a  $\lambda > 420 \text{nm}$  filter removes the UV light and a 150mm diameter,  $f=2\text{m}$  refractive lens refocuses the beam. Alternatively, a reflective-lens Cassegrain telescope is available for UV applications or to reduce chromatic aberrations. Visible optics divide the beam into parallel transmission lines leading to diagnostic end stations (Figure 1).

## PINHOLE CAMERA

The pinhole camera is calibrated in terms of  $\mu\text{m}/\text{pixel}$  with a USAF target positioned at the YaG crystal location. Vernier adjustments are made in-situ with a remote-control focus. Emittance is calculated from a look-up table of  $\epsilon$  vs.  $\sigma$  taking diffraction into account [1]. The diffraction resolution is approximately  $15 \mu\text{m}$  at 8keV photon energy.

In conjunction with the optical beam line and beam scraper systems, the pinhole camera will be used to study x-y coupling and beam lifetime as a function of single bunch current, total beam current, coupling correction scheme, accelerating voltage and ID configuration. Figure 2 shows an example of transverse beam size plotted as a function of global skew-quadrupole coupling correction prior to final optimization.

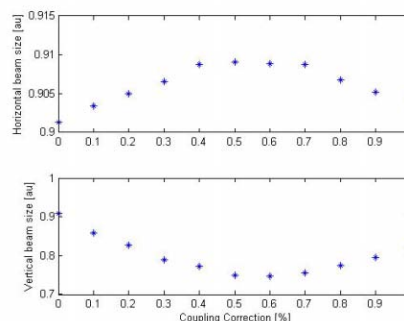


Figure 2: Beam size vs. coupling correction.

## VISIBLE/UV LIGHT MONITOR

Following the formalism of Hofmann [2], a software package was developed to propagate the angular spectral power density through the visible/UV beam line. At each element (cold finger, M0 mirror, windows, UV filter, etc) physical aperturing and/or frequency filtering is applied. The resulting radiation pattern is integrated to compute photon beam power or, in the case electric fields are used, polarization. Diffraction effects are not considered.

<sup>§</sup>Work supported by US Department of Energy  
Contract DE-AC02-76SF00515 and Office of Basic Energy Sciences,  
Division of Chemical Sciences.

Figure 3 shows the SR power distribution for  $\sigma$ -polarized light just after the cold finger and again as the beam emerges on the optical bench. The effect of the cold finger (cut through the center) and optical components (frequency filtering) are evident.

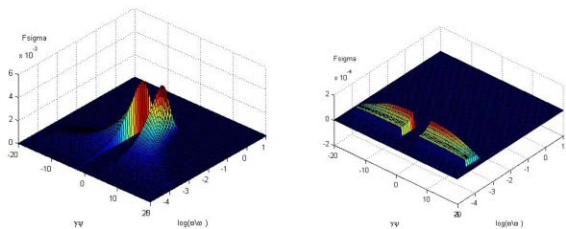


Figure 3: Angular spectral power density (a) at the dipole source and (b) filtered in the laboratory ( $\lambda > 420\text{nm}$ ).

Table 1 gives values for the photon beam power ( $\sigma + \pi$  modes) after various components in the beam line. By the time it reaches the laboratory, the beam power is reduced by a factor of  $10^{-5}$ . The current-normalized power is  $5\mu\text{W}/\text{mA}$  or, if we consider a single bunch, an energy of  $4\text{pJ}/\text{mA}/\text{pulse}$ . With a  $40\text{nm}$  FWHM filter centered at  $550\text{nm}$ , the beam power drops another factor of 200 to  $25\text{nW}/\text{mA}$  or  $20\text{fJ}/\text{mA}/\text{pulse}$ . Taking into account six 90%-transmission optical elements, the photon flux is  $\sim 3 \times 10^4$  photons/ $\text{mA}/\text{pulse}$  with the filter in place.

Table 1: Power in the visible/UV beam line ( $\mu\text{W}/\text{mA}$ ).

Source	Coldfinger	M0	Windows	UV block
$5 \times 10^3$	$3.8 \times 10^3$	$1.2 \times 10^3$	22	4.5

The first set of visible-light measurements included characterization of the un-focused light on a screen, passing the condensed beam through a glass prism (Figure 4) and imaging on a CCD camera [3]. Working in the visible spectrum, the diffraction limit for image resolution is only about  $50\mu\text{m}$ .

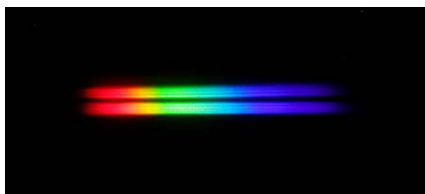


Figure 4: Visible beam spectrum - note cold finger slice through center.

The diagnostic program then moved directly to streak-camera bunch length measurements<sup>1</sup>. Figure 5 shows a plot of RMS bunch length plotted as a function of single-bunch current in the nominal SPEAR 3 optics (red dots). A fit of the natural RMS bunch length ( $\sigma_{z0}$ ) and inductive component of the effective impedance ( $Z/n_{\text{eff}}$ ) in the bunch-lengthening formula

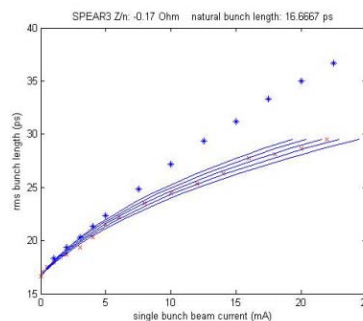


Figure 5: Curve fit to RMS bunch length vs. single-bunch current. The central curve has  $Z/n=0.17\Omega$ . The top and bottom curves have  $Z/n=0.19\Omega$  and  $0.15\Omega$ , respectively. The upper data (blue stars) is taken from tracking simulations in the SPEAR3 CDR.

$$\left( \frac{\sigma_z}{\sigma_{z0}} \right) - \left( \frac{\sigma_z}{\sigma_{z0}} \right)^3 = \frac{1}{\sqrt{2\pi}} \frac{\alpha_c I_b}{v_s^2 E / e} \left( \frac{R}{\sigma_{z0}} \right)^3 \cdot \text{Im} \left( \frac{Z_0^{\parallel}}{n} \right)_{\text{eff}}$$

yields  $\sigma_{z0}=16.7\text{ps}$  (nominal value  $16.6\text{ps}$ ) and  $\text{Im}\{Z/n_{\text{eff}}\} = 0.17\Omega$ . In this case, the RMS bunch length data was derived from FWHM as reported by the Hamamatsu streak camera software.

More technically, potential-well distortion leads to an asymmetric bunch length profile (Figure 6). Fitting the data to asymmetric Gaussian profiles produces RMS values that do not conform as well to the bunch-lengthening formula yet yield  $Z/n \sim 0.25\Omega$ . Either way, it is evident careful attention to broad-band impedance in SPEAR3 resulted in a ‘smooth’ (low-inductance) vacuum chamber.

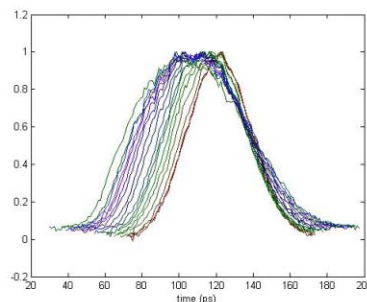


Figure 6: Asymmetric distortion of the bunch length profile at progressively higher single-bunch currents.

Bunch length measurements were also made during a series of low-alpha lattice experiments. SPEAR3 is somewhat unique in that the nominal momentum compaction factor ( $\alpha=0.0012$ ) leads to a relatively short natural bunch length of  $40\text{ps}$  FWHM ( $16.6\text{ps}$  RMS). Figure 7 contains a set of synchroscan streak-camera images taken with the momentum compaction reduced by a factor of 21. Progressing from left to right across the figure, the single-bunch current is increased from  $18\mu\text{A}$  to  $1000\mu\text{A}$  (not in equal increments).

<sup>1</sup>Hamamatsu C5680 on loan from LBL

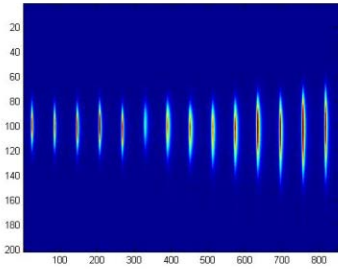


Figure 7: Streak camera images demonstrating bunch lengthening as a function of current with momentum compaction reduced by a factor of 21.

A comparison of streak camera images in the nominal optics with low-alpha optics is shown in Figure 8. A bunch length of 10ps FWHM is an important milestone because it provides potential to study relatively fast dynamical systems.

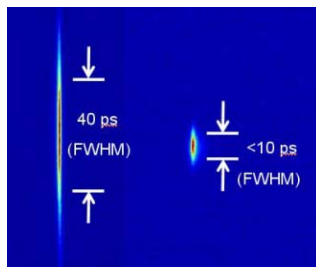


Figure 8: Comparison of single bunch image in nominal SPEAR 3 optics and  $\alpha/59$  optics.

Figure 9 shows a plot of FWHM bunch length vs. single bunch current with momentum compaction factor reduced by  $\alpha/21$  and  $\alpha/59$ . Based on these preliminary measurements, it should be possible to produce bunch lengths of 10ps FWHM with single bunch currents of order  $100\mu\text{A}/\text{bunch}$  (80pC), or about 30mA total beam current in 300 bunches. In parallel with the streak camera program, bolometer measurements showed some indication of THz SR ‘bursting’ at high single bunch currents [4].

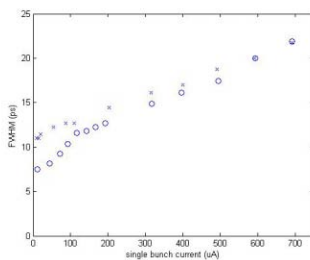


Figure 9: FWHM bunch length as a function of single bunch current for  $\alpha/21$  (x) and  $\alpha/59$  (o) optics.

## SUMMARY AND FUTURE

The pinhole camera and visible/UV beam line are now in operation as diagnostic tools for SPEAR3 yet both systems need further refinement to improve system flexibility and resolution. With 0.1% coupling, for instance, the vertical beam size is well below both the optical beam line resolution and even the pinhole camera resolution. Since the optical beam enters the laboratory unfocused, a two-slit interferometer may provide a solution. The 2ns-gate CCD camera [5] will add capability to monitor single-turn beam dynamics and to image the beam on a bunch-by-bunch basis. The addition of a dedicated streak camera would provide capability to study storage ring physics ranging from impedance measurements to collective instabilities and characterization of short-bunch dynamics.

## ACKNOWLEDGEMENTS

The authors would like to thank the SSRL technicians and summer students who contributed to the x-ray pinhole and synchrotron light monitor projects. A. Fisher, A. Lumpkin, J. Sebek and F. Sannibale made valuable contributions to the streak camera measurements and analysis. The low-alpha lattices were implemented by X. Huang, Y. Nosochkov and J. Safranek as part of an SSRL initiative to develop short-pulse capabilities at SPEAR3. Thanks to J. Bergstrom and A. Hofmann for interesting conversations on SR diagnostic systems.

## REFERENCES

- [1] J. Corbett, et al, ‘The SPEAR 3 Diagnostic Beamlines’, PAC 2005, Knoxville, TN, USA.
- [2] A. Hofmann, “The Physics of Synchrotron Radiation”, Cambridge University Press, 2004.
- [3] www.GreyPoint.com (Flea model).
- [4] Experiments performed by F. Sannibale on the SPEAR3 visible/UV diagnostic beam line.
- [5] Roper Scientific, PiMax Camera, UV enhanced, www.princetoninstruments.com.